ELSEVIER

Clinical Neurophysiology 112 (2001) 127–135

www.elsevier.com/locate/clinph

Estimating motor-unit architectural properties by analyzing motor-unit action potential morphology ☆

Zoia C. Lateva*, Kevin C. McGill

Rehabilitation Research and Development Center, VA Palo Alto Health Care System, 3801 Miranda Avenue/153, Palo Alto, CA 94304-1200, USA

Accepted 26 September 2000

Abstract

Objective: We investigated the architectural organization of groups of neighboring motor units (MUs) in normal brachial biceps and tibialis anterior muscles by analyzing morphological landmarks of their MU action potentials (MUAPs).

Methods: EMG signals containing multiple MUAPs were recorded using a monopolar needle electrode during moderate isometric voluntary contractions. The MUAPs were identified using computer-aided decomposition, and averaged. For each MUAP the onset, spike, terminal wave, and slow afterwave were identified; then the location of the MU's endplate and muscle/tendon junction were estimated from the latencies of the spike and terminal wave with respect to the MUAP onset.

Results: The analysis revealed a variety of architectural organizations, including single and multiple endplate zones, MU fractions, pennation, intramuscular aponeuroses, and centrally and non-centrally located endplates.

Conclusions: This type of morphological analysis of the MUAP promises to be informative for studying normal MU properties as well as evaluating MU reorganization in disease.

Keywords: Needle electromyography; EMG analysis; Motor unit; Motor unit action potential; Multi-MUAP analysis

1. Introduction

Studies based on biophysical models (Dimitrova, 1974; Gootzen et al., 1991) have shown that the potential field generated during the discharge of a motor unit (MU) evolves in 4 stages that correspond to 4 stages of electrical activity in the muscle fibers (Lateva et al., 1996; Lateva and McGill, 1998) (Fig. 1). First, the initiation of excitation at the muscle-fiber endplates produces a standing quadrupole wave. Second, the propagation of the two waves of excitation along the fibers produces two traveling quadrupole waves. Third, the termination of the two waves of excitation at the muscle/tendon junctions (MTJs) produces two standing dipole waves. These may or may not overlap in time, depending on the relative distances of the MTJs from the endplate. And fourth, the slow repolarization phase of the muscle fibers produces a weak standing quadrupole wave. These four stages are present in both voluntary and evoked MU discharges. Their timing depends on the muscle-fiber conduction velocity, endplate locations, and fiber lengths.

The motor-unit action potential (MUAP) recorded by a monopolar electrode is a temporal record of the above mentioned sequence of events. Although the exact shape of the MUAP waveform is different at different recording sites, depending on the location of the site with respect to the endplates, MTJs, and MU cross section, every MUAP waveform has certain specific morphological features that correspond to the 4 stages of electrical activity. While certain of these features sometimes have small amplitudes, they can usually be identified accurately after averaging. Analysis of these features can provide useful information about the anatomical characteristics of the MU (e.g. Lateva and McGill, 1999). Furthermore, analysis of multiple MUAPs recorded from a single site allows investigation of the architectural organization of neighboring MUs.

This paper uses these ideas to analyze and interpret MUAP waveforms from three architecturally different muscles.

2. Materials and methods

2.1. Computer simulations

Computer simulations were used to elucidate the relationship between the electrophysiological and anatomical characteristics of the MU and the morphological features of the

☆ Presented in part at the 11th International Congress of Electromyography and Clinical Neurophysiology, Prague, Czech Republic, 1999.

* Corresponding author. Tel.: +1-650-493-5000 ext. 63048; fax: +1-650-493-4919.

E-mail address: lateva@rrd.stanford.edu (Z.C. Lateva).

1388-2457/01/$ - see front matter CLINPH 2000088
PII: S1388-2457(00)00495-8

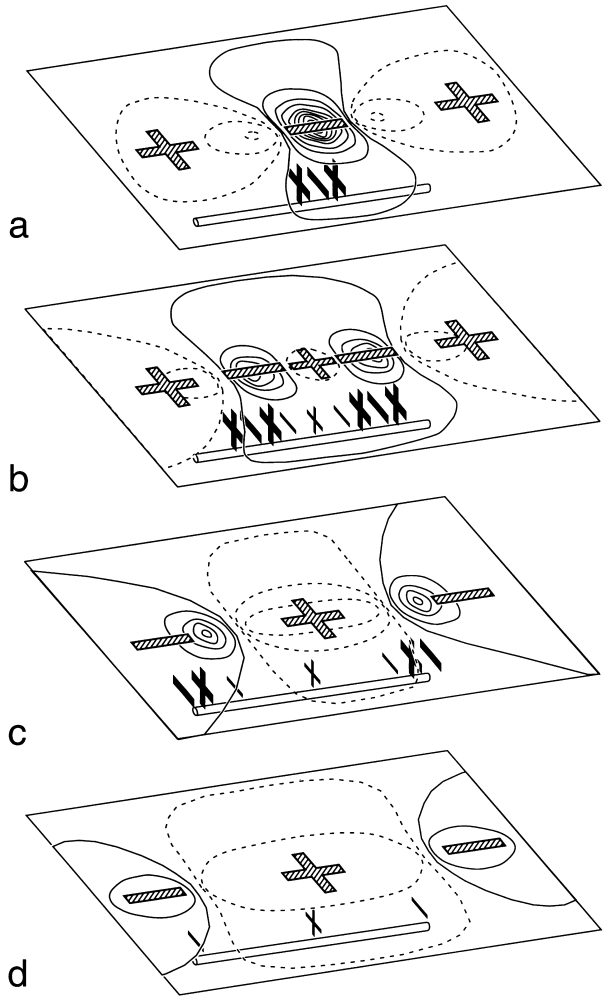

Fig. 1. The extracellular potential field during a MUAP evolves in four stages: (a) initiation, (b) propagation, (c) termination, and (d) slow repolarization. The transmembrane current sources along the muscle fibers are represented by the filled '+' and '−' symbols: the larger symbols correspond to the waves of excitation, the smaller ones to the slow repolarization. The polarities of the field are shown by the cross-hatched '+' and '−' symbols. The source configuration '+−+' is called a linear quadrupole source, and the corresponding field configuration '+−+' is called a quadrupole field. The source configurations '+−' and '−+' are called dipole sources, and the corresponding field configurations '+−' and '−+' are called dipole fields. (Quadrupole sources could equally well be indicated by '+− −+' to emphasize the fact that they are equivalent to pairs of dipole sources.)

MUAP. The MUAP was simulated as the convolution of a source function related to the intracellular action potential (IAP) and a weighting function related to the MU architecture. The IAP consisted of a spike and a slow repolarization phase. IAP parameters included the area of the spike and the amplitude and time constant of the slow repolarization phase. Weighting function parameters included the range of muscle-fiber semilengths (i.e. endplate-to-tendon lengths), the muscle-fiber conduction velocity, the muscle anisotropy, and the axial and radial distance of the electrode from the endplate. Parameters affecting only the absolute amplitude of the MUAP, including the intracellular and extracellular conductivities, the muscle-fiber diameters, and the innervation ratio, were not considered.

2.2. EMG recording

Ten normal volunteers (6 male and 4 female) aged 20–46 years (mean 33) with no history of neuromuscular disease gave their informed consent to participate in the experiments. The experimental procedures were approved by the Stanford University Committee on the Use of Human Subjects in Research.

EMG signals were recorded from brachial biceps (BB), tibialis anterior (TA), and first dorsal interosseous (FDI) muscles. The signals were recorded using monopolar needle electrodes and a remote surface reference electrode during moderate (<30% MVC), voluntary, isometric contractions. The electrodes were inserted at random locations into the muscle belly and adjusted to produce crisp sounding signals. The signals were amplified (TECA AA6) with filter settings at 8 Hz and 8 kHz, sampled at 10 kHz for a duration of 10 s, and then transferred to a Macintosh computer for further analysis.

2.3. MUAP identification and analysis

MUAPs were identified and averaged using an interactive computer-aided decomposition program that we have developed (McGill and Lateva, 1999). For identification, the EMG signals were digitally high-pass filtered at 600 Hz or 1.2 kHz to accentuate the MUAP spikes. The spikes were then classified into trains on the basis of their shapes and firing patterns. An experienced operator supervised each decomposition, ensuring full and correct identifications. Decomposition accuracy was judged by the regularity of the identified firing patterns and the amplitude of the residual noise. After identification, the MUAP waveforms were averaged from the original (i.e. not digitally filtered) EMG signal using the identified firing times as triggers. An algorithm was used to cancel the interference caused by the other identified MUAPs (McGill et al., 1985), yielding MUAP averages with noise levels typically less than 5 μV RMS.

3. Results

3.1. Computer-simulated MUAPs

Fig. 2 shows simulated MUAPs from 3 different recording sites: at the endplate, midway between the endplate and the MTJ, and at the MTJ. The MUAPs had three characteristic shapes: biphasic (initially negative), triphasic, and biphasic (initially positive), respectively. Despite the different shapes, each the MUAPs had morphological features that corresponded to the four stages of electrical activity.

Each MUAP had an abrupt onset at the time at which

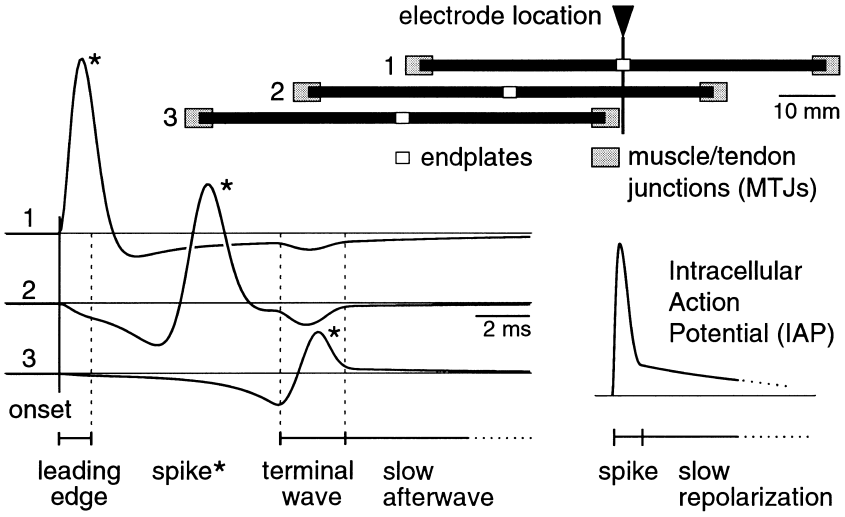

Fig. 2. Computer simulation. Simulated MUAPs from three MUs recorded at different axial locations. The architectural arrangement of the MUs and the location of the electrode are shown schematically. The intracellular action potential was modeled with a slow repolarization phase. The muscle-fiber conduction velocity was 4 m/s.

excitation was initiated at the endplate. Signals 2 and 3 of Fig. 2 had a distinct 'leading edge' which extended from the onset to a characteristic change in slope about 1.5 ms later. Each MUAP had a single negative peak or 'spike' corresponding to the propagation of the wave of excitation past the recording site. Each MUAP also had a distinct terminal wave at the time at which the wave of excitation terminated at the MTJ. At recording sites beyond the MTJ (Fig. 2, signal 3) the terminal wave changed from positive-going to negative-going and coincided with the spike.After the terminal wave, each MUAP slowly returned to the baseline with a 'slow afterwave' which followed the same time course as the slow repolarization component of the IAP.

3.2. Experimentally recorded MUAPs

Using computer-aided decomposition, we were able to identify and average 4–12 (mean 8) MUAPs from each experimentally recorded EMG signal. The onset, spike, terminal wave, and slow afterwave of each MUAP were identified by inspection. The MUAPs from each recording were then aligned by their onsets and grouped by morphological similarity. The architectural properties of each MU were estimated from the latencies of the MUAP features, assuming a conduction velocity of 4 m/s. Specifically, the endplate-to-electrode and endplate-to-MTJ distances were estimated from the onset-to-spike and onset-to-terminal-wave latencies, respectively. In some cases it was not possible to estimate the distant semilength reliably.

3.2.1. Initiation

In most of the signals, the MUAP averages had sufficiently high signal-to-noise ratios so that their onsets could be reliably distinguished from the baseline noise. Those signals in which the MUAP onsets could not be distinguished were not further analyzed.

All the MUAPs that began with an initial positive phase had a distinct leading edge with the same duration (about 1.5 ms) and characteristic shape as in the simulations. This similarity is shown in Fig. 3 (right), in which the leading edges of several MUAPs are plotted normalized to the same amplitude. In MUAPs recorded very near the endplate, the leading edge was obscured by the MUAP spike.

3.2.2. Spike

Most of the MUAPs had a single main spike. Some spikes had multiple peaks, undoubtedly reflecting unfused contributions from separate fibers with slightly different endplate locations or conduction velocities.

Comparing the spike latencies of MUAPs in different recordings revealed a variety of architectural organizations. In some recordings, such as Fig. 3, all the MUAPs had approximately the same spike latency, indicating that the endplates of these MUs all fell within a single zone. In other recordings, the MUAPs had different spike latencies. For example, the MUAPs in Fig. 4a fell into two groups with different spike latencies. The endplates of these MUs fell in two zones separated by about 8 mm. Interestingly, one of the MUAPs had two spikes, one occurring at each latency. This MU evidently was composed of two fractions, one fraction innervated in one zone and one in the other.

Other recordings revealed even more complex architectures. The MUAPs in Fig. 4b exhibited a large range of spike latencies, indicating a broad endplate zone extending over about 20 mm. The MUAPs in Fig. 5 included both triphasic and biphasic (initially positive) waveforms. In this case the electrode was evidently located between the

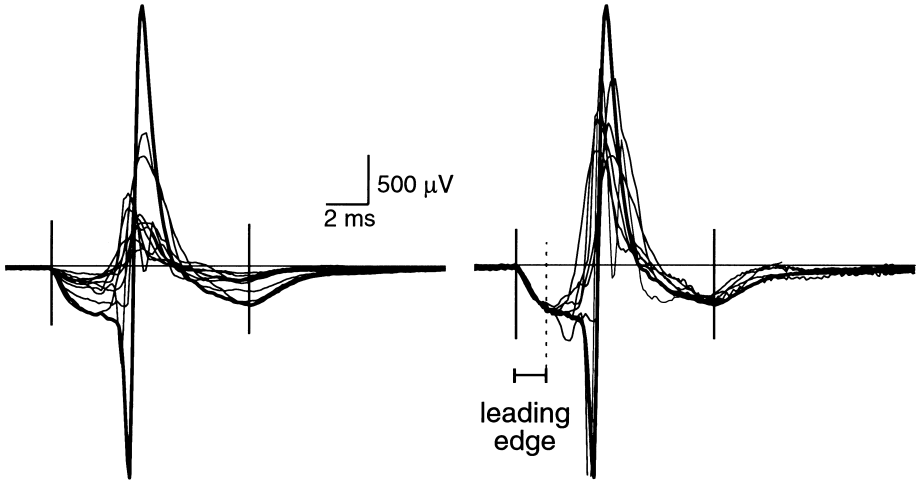

Fig. 3. MUAP initiation. Eleven MUAPs recorded from a single site in TA (left). The MUAPs were scaled (right) using factors 1 (highlighted) to 6.5 to show the similarity in the shapes of the leading edges. Note also the similarity in the amplitudes and shapes of the terminal waves after the scaling.

endplate and MTJ of the first group of MUs, and beyond the MTJ of the second group.

3.2.3. Terminal waves

Every MUAP had one or two terminal waves. MUAPs with two distinct terminal waves were seen only occasionally, and only in signals that had been recorded fairly near the endplate, as in Fig. 6a. These MUs had different semilengths, i.e. the endplate zone was closer to one MTJ than to the other. The terminal wave with the larger amplitude corresponds to the MTJ closer to the electrode.

Most of the MUAPs had only one noticeable terminal wave. The detection of only one terminal wave can mean either that the waves from the two MTJs occurred at the same time and superimposed, or that one of the waves failed to be detected. For MUAPs recorded near the endplate, such as those in Fig. 6b, the former situation is most likely, since the waves from both MTJs should have comparable amplitudes. Those MUs must therefore have had equal semilengths. However, for MUAPs recorded nearer one of the MTJs, such as those in Fig. 4a,b, the wave from the distant MTJ may have been too small to detect, especially if it were superimposed on the spike. For those MUAPs it was not possible to estimate the more distant semilength.

All the MUAPs from a given recording always had approximately the same terminal-wave latencies, even when there were differences in endplate locations (e.g. Fig. 4b). However, there were significant differences in terminal-wave latencies between muscles. Terminal wave latencies were much shorter in FDI than in BB and TA (Fig. 7), as would be expected given the shorter muscle fibers in FDI.

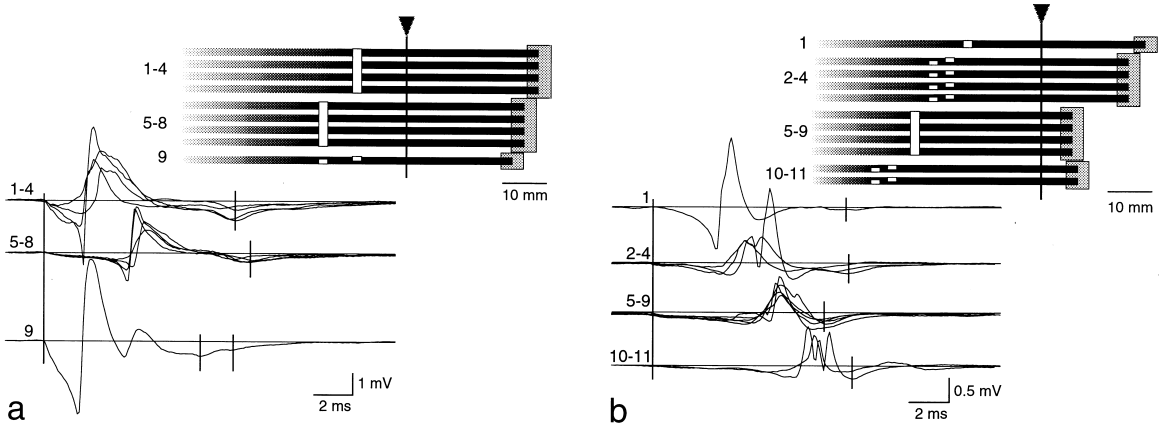

Fig. 4. (a) Two endplate zones, fractions. Nine MUAPs recorded from a single site in BB. The estimated architectural organization of the MUs is shown schematically. Two endplate zones can be distinguished. MU 9 has two fractions corresponding to the two endplate zones. The left semilengths could not be determined with confidence. (b) Pennation. Eleven MUAPs recorded from a single site in TA and the estimated MU architecture. The endplates are spread throughout a wide zone.

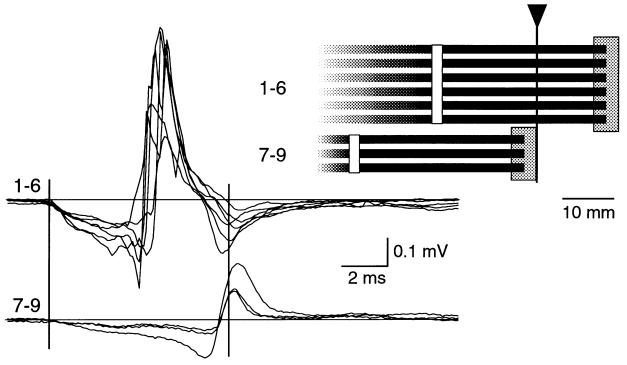

Fig. 5. Intramuscular aponeurosis. Nine MUAPs recorded from a single site in BB and the estimated MU architecture. The electrode is between the endplate and MTJ of one group of MUs but beyond the MTJ of the other.

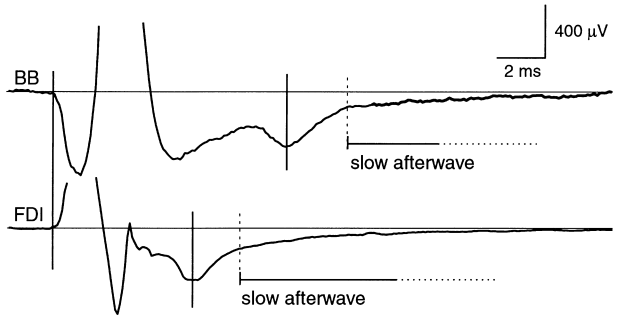

Fig. 7. MUAP duration. Two MUAPs recorded in BB and FDI. The terminal wave occurs later in BB because of the longer fiber lengths, but the overall durations are about the same (18 ms) because of the slow afterwaves.

3.2.4. Slow afterwave

The slow afterwave could be seen in almost all of the MUAPs, persisting for several milliseconds after the terminal wave. The slow afterwave was most pronounced in MUAPs recorded near the endplate and often was very small in MUAPs recorded midway between the endplate and the MTJ. It had an exponential shape with no distinct endpoint.

4. Discussion

Quantitative MUAP analysis is performed in clinical EMG to diagnose neuromuscular disorders (Stålberg et al., 1986, 1996; Daube, 1991). The analysis conventionally includes measurements primarily concerned with the MUAP spike, including amplitude, duration, area, number of phases, and number of turns. These measures have been shown empirically, and through computer simulations, to reflect MU remodeling associated with myopathic and neurogenic disorders. However, the physiological interpretations of these measures are not always straightforward.

The analysis presented here is based on the entire MUAP waveform, not just the spike. It involves identifying specific features of the MUAP that correspond to the four stages of electrical activity in the muscle fibers. The latencies of these features can be related to anatomical characteristics of the MU. The existence of the MUAP onset and terminal wave has been known for some time (Gydikov and Kosarov, 1972). However, these features often have small amplitudes and require noise-free baselines in order to be identified reliably. It has not been practical to obtain MUAP waveforms with sufficiently high signal-to-noise ratios in routine clinical studies, even with computerized averaging techniques. This is perhaps the main reason that little attention has been paid to these features in clinical analysis.

The MUAPs in this study were recorded using monopolar needle electrodes. Monopolar electrodes are more suitable than concentric electrodes for the type of analysis presented here. This is because the cannula of the concentric electrode makes a sizable contribution to the recorded signal (Stålberg et al., 1986, 1996). The size and shape of the cannula contribution depend on the location of the needle with respect to the MU and the volume conductor, and cannot readily be predicted (Dumitru and King, 1998). Moreover, the signal components that arise from distant sources, such as the initiation and terminal wave of the MUAP, tend to appear as common-mode signals to the concentric electrode and to be attenuated. MUAPs recorded by monopolar electrodes, on the other hand, have shapes very similar to those predicted by the mathematical models.

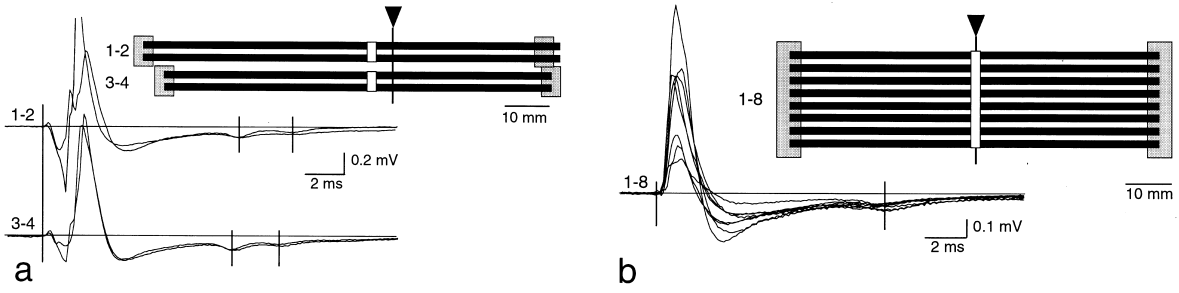

Fig. 6. (a) Asymmetrical semilengths. Four MUAPs recorded from a single site in BB and the estimated MU architecture. Both groups of MUs have two terminal waves, indicative of asymmetrical semilengths. (b) Symmetrical semilengths. Eight MUAPs recorded from a single site in BB and the estimated MU architecture. All the MUs have similar architectures. The presence of only one terminal wave points to symmetrical muscle-fiber semilengths.

The ability of the monopolar electrode to detect MUAP components arising from the endplate and the MTJ – which, in the case of a long muscle such as biceps, may be several centimeters from the electrode – can be attributed to several reasons. First, these components represent the summed activity of all the fibers of the MU. Second, electrical potentials attenuate less rapidly in the axial direction than in the radial direction because of the anisotropy of the muscle tissue (Geddes and Baker, 1967; Dimitrov and Dimitrova, 1974). Third, the terminal waves are produced by dipole, rather than quadrupole, sources (Dimitrova, 1974; Dumitru and King, 1991; Gootzen et al., 1991), the potentials of which attenuate less rapidly with distance than potentials of quadrupole sources (Plonsey, 1969). Finally, the components in question can be quite small, and careful signal averaging may be necessary in order to detect them.

The MUAP waveform is a record in time of electrical events that take place in time and space. The relationship is analogous to that involved in the sound perceived by a spectator during a marching band performance in a football stadium (cf. marching band analogy in Stålberg et al., 1996). Each spectator perceives a different sound intensity profile, depending on his or her location with respect to the band's trajectory. However, each hears the first and last notes of the performance at the same times as everyone else. In a similar way, the configuration of the MUAP spike is different at each recording site, but the timing of the onset and terminal wave are the same at all recording sites.

4.1. Initiation

Our results agree with those of other investigators that the MUAP has a distinct onset which corresponds to the onset of the depolarization of the muscle fibers at the endplates (Stålberg et al., 1986, 1996; Dumitru et al., 1999). Our simulations further show that MUAPs recorded at least 10 mm from the endplate have a characteristically shaped leading edge which reflects the development of the waves of excitation in the muscle fibers. Starting from the baseline, the potential increases in magnitude as the endplates depolarize, continues to increase as the two waves of excitation begin to emerge, and then tapers off once they have fully emerged. The leading edges of all the MUAPs we recorded had shapes that closely matched the shape predicted by the mathematical model.

The simulations show that the duration of the leading edge (from the MUAP onset to the change in slope) equals the sum of the duration of the IAP spike plus the amount of dispersion in the activation times of the individual fibers. All of the MUAPs we investigated had leading-edge durations of approximately 1.5 ms, which is very close to the duration of the IAP spike measured by Ludin (1969). This implies very little dispersion of activation times. Dispersion of activation times could arise due to differences in conduction times along the terminal nerve branches and due to differences in neuromuscular transmission delays. Terminal nerve branches are thought to differ in length by no more than about 2 mm (Stålberg and Trontelj, 1994), and axonal conduction velocities in terminal branches are about 12 m/s (Stålberg and Trontelj, 1970). Thus differences in terminal conduction times would be expected to be less than about 0.15 ms. Neuromuscular transmission jitter in normal muscle is usually less than 0.01 ms (Stålberg and Trontelj, 1994). Thus the dispersion of the activation times of the fibers of a normal MU should indeed be expected to be small compared to the duration of the IAP.

4.2. Spike

At recording sites near the endplate, the MUAP spike is produced by the development and emergence of the waves of excitation at the endplate. Along the length of the muscle fibers, the spike is due to the propagation of one of the waves of excitation past the electrode. At and beyond the MTJ, the spike merges with the terminal wave. The precise characteristics of the spike are thought to reflect primarily the contributions of the few fibers that lie closest to the electrode rather than the MU as a whole (Nandedkar et al., 1985, 1988). Our analysis is not based on any characteristic of the spike except for the latency of its peak, which is used to estimate the location of the electrode with respect to the MU endplate.

The risetime of the spike is generally thought to reflect the distance of the closest fibers from the electrode (Stålberg et al., 1986, 1996; Daube, 1991). We did not specifically take the spike risetimes into account. That is, we analyzed all the MUAPs that we were able to detect, without regard to their spike risetimes. Thus, some of the MUs we detected may not have had fibers quite as close to the electrode as others. However, the territories of all the MUs must have been fairly close to the electrode in order for them to have been detected at all, and it is therefore not unreasonable to consider them to be neighbors of one another.

4.3. Terminal waves

The terminal waves, or 'small positive afterwaves' (Stålberg et al., 1986, 1996), are produced when the waves of excitation reach the ends of the muscle fibers. This mechanism is described by the leading-trailing dipole model (Dumitru and King, 1991). During the propagation of the wave of excitation, the dipole moment of the transmembrane current sources associated with the leading wavefront is balanced by the dipole moment associated with the trailing wavefront. When the wave reaches the end of the fiber, however, the leading dipole disappears, leaving only the trailing dipole, which produces a dipole potential field in the volume conductor. This field, which is called the terminal standing wave, falls off less quickly with distance than the quadrupole field associated with propagating wave of excitation, and it is detected at the recording site as the terminal wave of the MUAP.

Terminal standing waves are produced at both ends of the

muscle. If the endplate is located midway between the two MTJs, these waves will occur at the same time, resulting in only a single terminal wave in the MUAP. If the endplate is located asymmetrically, the waves will occur at different times, resulting in two separate terminal waves in the MUAP. The latency of the terminal wave reflects the endplate-to-MTJ propagation time, and hence the muscle-fiber semilength. Our results found differences in semilengths between muscles, as would be expected (see also Dumitru and King, 1999), but no great differences in semilengths between the neighboring MUs at a particular site in the same muscle, even when the MUs had different endplate zones and insertion sites.

Our computer simulations show that the duration of the terminal wave equals the sum of the IAP spike duration plus the dispersion of the termination times of the individual fibers. This dispersion can arise because of differences in muscle-fiber semilengths and/or conduction velocities. Since muscle-fiber conduction velocities have been shown to vary by no more than about $\pm 15\%$ in an individual intact muscle (Buchthal et al., 1955; Buchthal and Sten-Knudsen, 1959), we believe that most of the dispersion is probably due to differences in semilengths. These differences would arise because of dispersion in the locations of the endplates and/or the tendon attachment sites of the individual fibers. Most of the MUAPs we analyzed had terminal waves with durations of 2–3 ms. Assuming an IAP duration of 1.5 ms, this would mean a dispersion of termination times of up to 1.5 ms, and hence a difference of up to 6 mm between the longest and shortest semilengths.

4.4. Slow afterwave

After the passage of the wave of excitation, the repolarization of the muscle-fiber membrane takes place in two phases. The first 80% of the repolarization takes place within 1 ms after the depolarization, but the remaining 20% takes place over a period lasting 10 ms or longer, which is referred to as the slow repolarization phase (Persson, 1963; Ludin 1969). Thus while the two waves of excitation are propagating, the length of fiber between them is undergoing slow repolarization. After the waves have terminated, the entire fiber undergoes slow repolarization. The small transmembrane currents associated with slow repolarization set up a weak quadrupole field in the volume conductor which is centered at the endplate (Lateva and McGill, 1998; McGill and Lateva, 2000).

Our computer simulations show that for MUAPs recorded near the endplate, a large part of the final positive phase of the MUAP is due to the field produced by the slow repolarization currents. For example, the final positive phases of the MUAPs in Fig. 6 can be interpreted in the following way. Immediately after the spike, the recorded potential is still influenced strongly by the quadrupole fields associated with the receding waves of excitation. As the waves get father away, though, their effect becomes smaller and the recorded potential is dominated by the field of the slow repolarization currents. Thus the smooth exponential parts of the final positive phases of the MUAPs in Fig. 6a and b, starting before the terminal waves and extending until the signals reach the baseline, are due to the slow repolarization and reflect its timecourse. The terminal waves are superimposed on this smooth exponential component.

While the parts of the MUAP before the terminal wave are influenced by both the propagating waves and the slow repolarization, the final return of the MUAP to the baseline after the terminal wave is due solely to the slow repolarization. We have used the term ‘slow afterwave’ to refer to this part of the signal, following Lang and Vaahtoranta (1973). The slow afterwave can be seen at all recording sites, although it is best seen at recording sites near the endplate, where the slow repolarization field is strongest. The slow afterwave can contribute substantially to the total duration of the MUAP, although, due to the lack of a distinct endpoint, measurement of duration is somewhat arbitrary. In particular, we found, as did Dumitru and King (1999), that the overall durations of MUAPs from FDI, BB, and TA are often comparable, despite differences in muscle-fiber length, due to the presence of the slow afterwave.

4.5. Comparative motor-unit architecture

Using the latencies of the MUAP spike and terminal waves with respect to the onset, we were able to estimate the location of the MU endplate and MTJ with respect to the electrode. Furthermore, by analyzing multiple MUAPs from the same recording, we were able to compare the architectural organization of multiple neighboring MUs.

In BB, groups of neighboring MUs tended to have very similar architectures. That is, the endplates were all located in the same zone and the semilengths were similar. This is consistent with BB’s known parallel-fibered architecture with most of the fibers extending over the entire length of the muscle. In some recordings, however, two distinct endplate zones could be distinguished (Fig. 4a), which is consistent with previous observations of existence of multiple endplate zones in BB (Buchthal et al., 1955; Christensen, 1959; Aquilonius et al., 1984; Masuda et al., 1985). Of the MUs in Fig. 4a, all were fully innervated in one zone or the other, except for one MU which was innervated in both zones. In another recording (Fig. 5), the electrode was found to have been between the endplate and MTJ of one group of MUs but beyond the MTJ of another group. This arrangement is consistent with an intramuscular aponeurosis, in which the MUs in the first group run parallel to the aponeurosis while the MUs in the second group insert onto it. The existence of such an aponeurosis in the distal part of BB has been demonstrated in ultrasound imaging studies (Papas, 1999).

In TA, some groups of neighboring MUs were quite homogeneous (e.g. Fig. 3), while other groups were very

different (e.g. Fig. 4b). In the latter case, the electrode was apparently in a pennate part of the muscle, so that it was closer to the endplates of some of the MUs and closer to the MTJs of others. Such an arrangement is consistent with the TA's known bipennate architecture and superficially distributed endplates (Christensen, 1959; Aquilonius et al., 1984). Further work is needed to map out the differences in architectural organization throughout the entire muscle.

It should be pointed out that the estimation of these architectural properties requires an estimate of muscle-fiber conduction velocity. We assumed that every MU in each recording had the same conduction velocity, 4 m/s, a typical mean value measured during voluntary contractions (Buchthal et al., 1955; Buchthal and Sten-Knudsen, 1959; Stålberg, 1966). It is known that the actual conduction velocities of MUs from the same muscle can differ by up to $\pm 15\%$, and so our distance estimates are probably accurate only to about this same level. However, since the differences in endplate-to-electrode distance estimated for some groups of MUs were often much greater than this, we believe that the major features of the architectural organizations presented here are substantially correct.

It is also of interest to consider the amplitudes of the leading edge and the terminal wave. The results of our computer simulations show that if the electrode is relatively far from the endplate, and thus approximately equidistant from the endplates of all the fibers of the MU, then the amplitude of the leading edge is proportional to the number of fibers (i.e. to the innervation ratio). Therefore, for multiple MUAPs recorded at the same distance from their endplates, the relative amplitudes of the leading edges can be taken as an index of the relative innervation ratios of the MUs. For example, based on the amplitudes of their leading edges, the MUs in Fig. 3 can be estimated to have innervation ratios that vary by a factor of 6.

The computer simulations also predict the amplitude of the terminal wave to be proportional to the innervation ratio, as long as the electrode is not too close to the MTJ. For example, the MUs in Fig. 6b have roughly equal terminal-wave amplitudes, and so evidently have roughly equal innervation ratios. Moreover, the terminal waves of the MUAPs in Fig. 3 have the same relative sizes as the leading edges, as would be expected if both the leading-edge and terminal-wave amplitudes were proportional to the innervation ratio.

4.6. Final comments

The method we have presented – of analyzing morphological features of multiple, concurrently active MUAPs from a single recording – is, as far as we know, the only method currently available for investigating the architectural organization of groups of neighboring MUs in vivo. The approach is made possible by software we have developed which enables full decomposition of multiunit EMG signals into their constituent MU trains and high signal-to-noise-ratio averaging of the MUAP waveforms. The method could also be extended to analyze MUAPs recorded concurrently from different sites in the muscle, allowing multiple views of the same MUs and hence a more complete description of the muscle architecture. This type of analysis promises to be informative for several applications, including interpretation of clinically measured MUAP parameters, biomechanical modeling of force production, and evaluation of MU reorganization in aging and disease.

Acknowledgements

This study was supported by the Medical and Rehabilitation Research and Development Services of the U.S. Department of Veterans Affairs.

References

Aquilonius SM, Askmark H, Gillberg PG, Nandedkar S, Olsson Y, Stålberg E. Topographical localization of motor endplates in cryosections of whole human muscles. Muscle Nerve 1984;7:287–293.

Buchthal F, Guld C, Rosenfalck P. Innervation zone and propagation velocity in human muscle. Acta Physiol Scand 1955;35:174–190.

Buchthal F, Sten-Knudsen O. Impulse propagation in striated muscle fibers and the role of the internal currents in activation. Ann NY Acad Sci 1959;81:422–445.

Christensen E. Topography of terminal motor innervation in striated muscles from stillborn infants. Am J Phys Med 1959;38:65–78.

Daube JR. AAEM minimonograph #11. Needle examination in clinical electromyography. Muscle Nerve 1991;14:685–700.

Dimitrov GV, Dimitrova NA. Extracellular potential field of an excitable fibre immersed in anisotropic volume conductor. Electromyogr Clin Neurophysiol 1974;14:437–450.

Dimitrova N. Model of the extracellular potential field of a single striated muscle fibre. Electromyogr Clin Neurophysiol 1974;14:53–66.

Dumitru D, King JC. Far-field potentials in muscle. Muscle Nerve 1991;14:981–989.

Dumitru D, King JC. Concentric needle recording characteristics related to depth of tissue penetration. Electroencephalogr Clin Neurophysiol 1998;109:124–134.

Dumitru D, King JC. Motor unit action potential duration and muscle length. Muscle Nerve 1999;22:1188–1195.

Dumitru D, King JC, Rogers WE. Motor unit action potential components and physiologic duration. Muscle Nerve 1999;22:733–741.

Geddes LA, Baker LE. The specific resistance of biological material – a compendium of data for the biomedical engineer and physiologist. Med Biol Eng 1967;5:271–293.

Gootzen TH, Stegeman DF, Van Oosterom A. Finite limb dimensions and finite muscle length in a model for the generation of electromyographic signals. Electroencephalogr Clin Neurophysiol 1991;81:152–162.

Gydikov A, Kosarov D. Extraterritorial potential field of impulses from separate motor units in human muscles. Electromyogr Clin Neurophysiol 1972;12:283–305.

Lang AH, Vaahtoranta KM. The baseline, the time characteristics and the slow after-waves of the motor unit potential. Electroencephalogr Clin Neurophysiol 1973;35:387–394.

Lateva ZC, McGill KC. The physiological origin of the slow afterwave in muscle action potentials. Electroencephalogr Clin Neurophysiol 1998;109:462–469.

Lateva ZC, McGill KC. Satellite potentials of motor unit action potentials in normal muscles: a new hypothesis for their origin. Clin Neurophysiol 1999;110:1625–1633.

Lateva ZC, McGill KC, Burgar CG. Anatomical and electrophysiological determinants of the human thenar compound muscle action potential. Muscle Nerve 1996;19:1457–1468.

Ludin HP. Microelectrode study of normal human skeletal muscle. Eur Neurol 1969;2:340–347.

Masuda T, Miyano H, Sadoyama T. The position of innervation zone in the biceps brachii investigated by surface electromyography. IEEE Trans Biomed Eng 1985;32:36–42.

McGill KC, Lateva ZC. Accurate estimation of motor-unit action potential waveforms and discharge patterns. Clin Neurophysiol 1999;110(Suppl 1):250–251.

McGill KC, Lateva ZC. Slow repolarization phase of the intracellular action potential influences the motor unit action potential. Muscle Nerve 2000;23:826–827.

McGill KC, Cummins KL, Dorfman LJ. Automatic decomposition of the clinical electromyogram. IEEE Trans Biomed Eng 1985;32:470–477.

Nandedkar S, Sanders D, Stålberg E. Selectivity of the EMG recording techniques: a simulation study. Med Biol Eng Comput 1985;23:536–540.

Nandedkar S, Sanders D, Stålberg E, Andreassen S. Simulation of concentric needle EMG motor unit action potentials. Muscle Nerve 1988;11:151–159.

Papas G. Characterization of biceps brachii architecture and contraction mechanics using medical imaging techniques. PhD thesis, Stanford, CA: Stanford University, 1999.

Persson A. The negative after-potential of frog skeletal muscle fibers. Acta Physiol Scand 1963;58(Suppl):205.

Plonsey R. Bioelectric phenomena, New York: McGraw-Hill, 1969.

Stålberg E. Propagation velocity in human muscle fibers in situ. Acta Physiol Scand 1966;70(Suppl):287.

Stålberg E, Trontelj JV. Demonstration of axon reflexes in human motor nerve fibers. J Neurol Neurosurg Psychiatry 1970;33:571–579.

Stålberg E, Trontelj JV. Single fiber electromyography, New York: Raven, 1994.

Stålberg E, Andreassen S, Falck B, Lang H, Rosenfalck A, Trojaborg W. Quantitative analysis of individual motor unit potentials: a proposition for standardized terminology and criteria for measurement. J Clin Neurophysiol 1986;3:313–348.

Stålberg E, Nandedkar SD, Sanders DB, Falck B. Quantitative motor unit potential analysis. J Clin Neurophysiol 1996;13:401–422.